Journal of Materials Chemistry A

PAPER

View Article Online
View Journal | View Issue

Cite this: J. Mater. Chem. A, 2016, 4, 16507

Soybean-derived hierarchical porous carbon with large sulfur loading and sulfur content for high-performance lithium–sulfur batteries†

Guofeng Ren,[a] Shiqi Li,[a] Zhao-Xia Fan,[b] Juliusz Warzywoda[c] and Zhaoyang Fan*[a]

An hierarchical porous carbon nanostructure with intrinsic O- and N-dopants and an ultrahigh specific surface area of 1500 m^2 g^{-1} is reported towards the goal of designing and achieving a better sulfur electrode for lithium–sulfur batteries (LSBs) that can provide both large sulfur loading and large sulfur content and are based on a facile fabrication process. This nanostructure was derived from crude soybeans in a facile pyrolysis process. Using it as a sulfur host, the S/C active composite with 80% sulfur content was made. Cells with different sulfur loadings were investigated and were found to demonstrate large capacity, high coulombic and energy efficiencies, and high cycling stability. In particular, for a sulfur loading of 5.5 mg cm^{-2} and a sulfur content of 80%, cells displayed a specific capacity of *ca.* 950 mA h g^{-1}, which corresponds to an areal capacity of 5.2 mA h cm^{-2}. Such a performance moves LSB technology closer to practical applications.

Received 29th August 2016
Accepted 17th September 2016

DOI: 10.1039/c6ta07446d

www.rsc.org/MaterialsA

1. Introduction

To meet the insatiable demands for energy storage, new battery technologies are under intensive investigation. Considering their potential to provide an energy density of 2600 W h kg^{-1}, 3–5 times that of the conventional Li-ion batteries, and the low cost and environmental friendliness of sulfur, lithium–sulfur batteries (LSBs) are particularly attractive.[1–7] The insulating nature of sulfur and the reduction products (Li_2S_2 and Li_2S) prefer a catholyte chemistry, in which the reduction intermediates (lithium polysulfides) are soluble. This enables a solid–liquid–solid conversion in the entire electrochemical process and therefore, overcomes the otherwise slow kinetics in a solid–solid reaction.[8] However, the soluble polysulfides may shuttle between and react on the cathode and the anode, causing a chemical shortcut in the cell[9,10] and thus giving rise to the irreversible loss of active materials, capacity fade, anode corrosion, low coulombic efficiency and self-discharge.[1,11] Such a shuttle effect, as well as other effects, prevent LSBs from achieving a large capacity with a reasonable cycling stability.

Steady progress has been made to advance LSB technology in recent years through cathode nanostructure engineering,[12–16] new electrolyte chemistry,[17,18] and lithium anode passivation,[19–21] among others. In terms of the cathode design aimed to diminish the adverse shuttle effects, the nanostructured conductive hosts, particularly carbonaceous nanomaterials,[13,22,23] have been well studied to physically prevent the soluble lithium polysulfides from migrating out of the cathode.[14,16] More recently, chemical immobilization of polysulfides through chemisorption[24,25] has been found to be more effective to achieve this goal. For the nonpolar carbonaceous surfaces, heteroatom nitrogen doping,[26,27] metal oxides,[28–30] or polymers[31] are commonly used for chemisorption of lithium polysulfides that have a polar nature.[32] Significant progress has been made toward the practical application of LSBs.[33–35]

As emphasized in ref. 8, a practical battery electrode must have an areal capacity of a few mA h cm^{-2}, and the electrode material must be cost-effective. However, a considerable number of the recently reported electrode structures is based on very complex fabrication processes; and hence, is not cost effective. Whereas, the structures based on facile processes simply cannot offer a reasonable performance. Furthermore, many reports show good performance, but use the structures with a small sulfur loading, and, in particular, with a small sulfur content in the active S/C composite. This results in a volumetric capacity, a very critical parameter for a battery, even lower for the LSBs than for the traditional Li-ion batteries. In this study, we endeavor to solve these problems by developing a facile process for fabrication of the cathode structure that offers impressive performance. Hierarchical porous carbon, intrinsically doped with nitrogen and oxygen, was prepared using crude soybeans, which inherently contain nitrogen and oxygen, as a precursor in a facile activation process

[a]Department of Electrical and Computer Engineering and Nano Tech Center, Texas Tech University, Lubbock, Texas 79409, USA. E-mail: zhaoyang.fan@ttu.edu
[b]School of Mechanical Engineering, Beijing Institute of Technology, Beijing 100081, China
[c]Materials Characterization Center, Whitacre College of Engineering, Texas Tech University, Lubbock, Texas 79409, USA

† Electronic supplementary information (ESI) available. See DOI: 10.1039/c6ta07446d

involving mixing with KOH and pyrolysis in Ar. The resulting carbonaceous material displays a hierarchical porous structure with an ultrahigh specific surface area of *ca.* 1500 $m^2 g^{-1}$. Using it as sulfur host, the S/C composite with high sulfur content (80%) was made. Cells with different sulfur loadings were investigated, demonstrating good capacity and cycling stability. In particular, for a sulfur loading of 5.5 mg cm^{-2} and a sulfur content of 80%, cells displayed a specific capacity of *ca.* 950 mA h g^{-1} at 0.2C. This corresponds to an areal capacity as high as 5.2 mA h cm^{-2}, which is comparable to the reported performance of the state-of-the-art LSBs but prepared *via* a complex fabrication process.[24,36]

2. Results and discussion

The schematic in Fig. 1a illustrates the entire process to produce the S/C composite. Crude soybeans, without being crushed into powder, were directly used as a doped carbon precursor. Soybeans mainly consist of protein (36%), carbohydrates (30%), and soybean oil (20%), with the remainder being water and ash. The protein- and carbohydrate-rich soybeans provide nitrogen and oxygen sources for the doped carbon material. After hydrothermally pretreating crude soybeans at 180 °C for 20 hours, a black thick oil-like paste was obtained. The scanning electron microscope (SEM) image of the paste (Fig. S1 in the ESI†) reveals a morphology similar to a thick oil mixed with the irregularly-shaped larger particles. The crude soybeans were essentially disintegrated and liquefied in this process, resulting in a dispersion of carbonaceous intermediates. This pretreatment not only converts the solid soybeans into a dispersible paste for easy mixing with KOH in the subsequent step for activation, but is also critical for the creation of the C=C backbone for the final activated carbon product.[37,38] The oil-like paste, after being well mixed with KOH to form a slurry, was then activated at 800 °C in the argon environment by a pyrolysis and corrosion process, to obtain the final soybean-derived carbonaceous material. This material was then employed as a conductive matrix that was mixed with sulfur powder to obtain the S/C mixture with sulfur mass ratio as high as 80% in the active S/C composite.

The morphology and microstructure of the final carbonaceous material was investigated by scanning electron microscopy (SEM) and transmission electron microscopy (TEM) to reveal its hierarchical porous structure. As shown in the SEM image in Fig. 1b, the strategy of hydrothermal pretreatment followed by pyrolysis in the presence of KOH activation agent

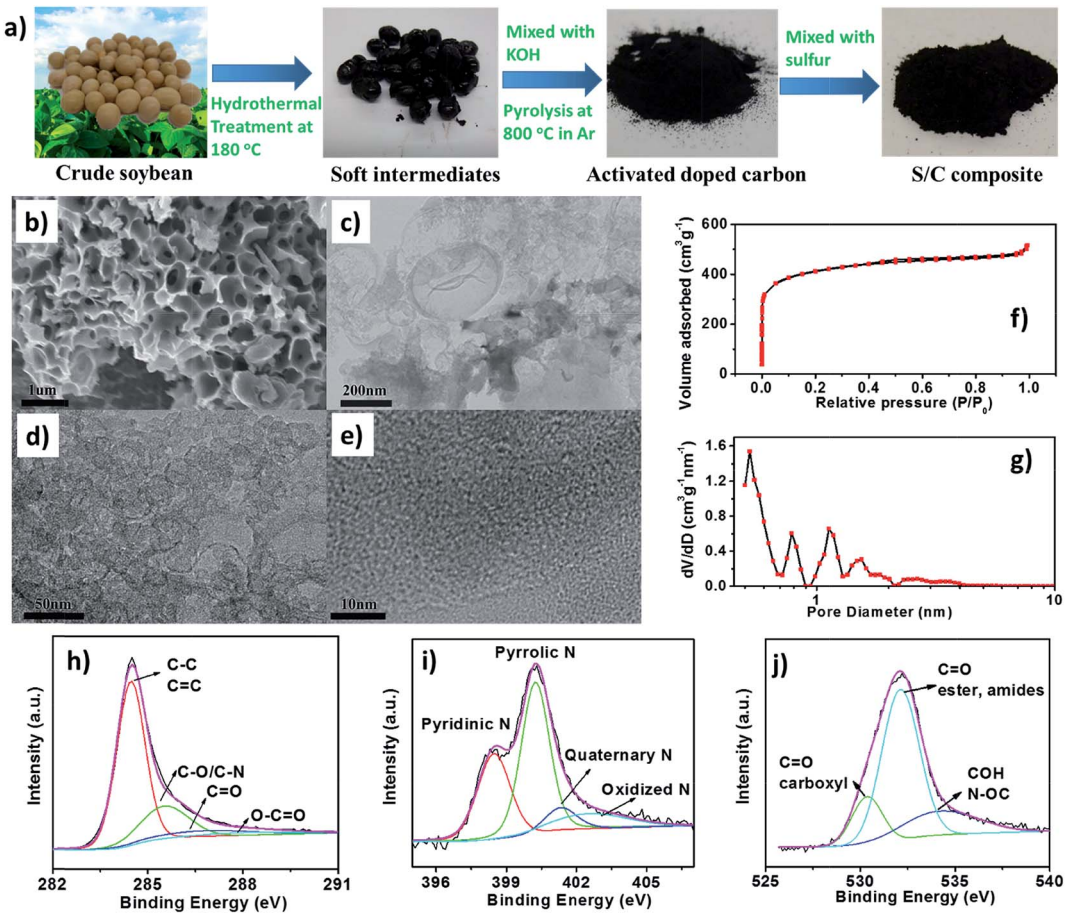

Fig. 1 (a) Schematic of the process of the preparation of the S/C composite; (b) SEM image and (c–e) TEM images of the carbonized material; (f) nitrogen adsorption–desorption isotherm and (g) pore size distribution of the soybean-derived porous carbon; (h) C 1s, (i) N 1s, and (j) O 1s XPS spectra of the hierarchical carbon.

transforms the soybean solid into a three dimensional (3D) bicontinuous porous structure. Such a bicontinuous pore morphology consists of the hollow, micrometer- or sub-micrometer-sized spheres that are embedded inside the structure, forming a nest, and are interconnected through the smaller pores that interpenetrate through the thin shells of spheres. This creates a hierarchical porous structure at the micro-scale. It is believed that the C=C backbone, created in the hydrothermal pretreatment process, has the tendency to fold into microspheres at higher temperatures in the pyrolysis process, while KOH-induced etching tends to disrupt the structure by forming a bicontinuous structure.[38] A similar hierarchical structure was also formed at the nanoscale, as revealed by the TEM images at different magnifications in Fig. 1c and d. The hollow spheres have a diameter distribution ranging from hundreds of nanometers to tens of nanometers or even smaller sizes. The pores are interconnected in a 3D structure with the smaller pores nested inside the larger pores. The high-resolution TEM image in Fig. 1e suggests that the micropores with a diameter of less than 2 nm are present on the carbon surface.

To further quantify the obtained porous structure, the nitrogen adsorption isotherm was acquired using a micropore analyzer (Fig. 1f). The prominent nitrogen uptake at a relative pressure (P/P_0) below 0.01 is due to micropores, whereas the uptake at $P/P_0 = 0.05$–0.3 is due to mesopores. The N_2 adsorption with a plateau at higher relative pressures followed by an increase at $P/P_0 > 0.9$ reveals the presence of large mesopores and macropores.[39] The pore size distribution was calculated from the nitrogen adsorption data (Fig. 1g), which clearly shows the presence of both micro- and meso-pores, and confirms the hierarchical porous structure of the obtained material. The cumulative pore volume plot (Fig. S2†) shows that micropores, defined as pores with a diameter smaller than 2 nm, contribute most of the total pore volume of *ca.* 0.7 $cm^3\ g^{-1}$. The Brunauer–Emmett–Teller (BET) specific surface area (S_{BET}) was found to be *ca.* 1500 $m^2\ g^{-1}$. Such a hierarchical microporous/mesoporous structure is known to be effective for physically trapping the soluble polysulfides in the sulfur electrode, as well as for rapid Li^+ transportation.

The structure, elemental composition and chemical bonding in the obtained porous structure were studied. The Raman spectrum shows two typical carbon peaks at *ca.* 1345 cm^{-1} and *ca.* 1590 cm^{-1} (Fig. S3a†). The intensity of the defect-induced D peak at *ca.* 1345 cm^{-1} is stronger than that of the G peak at *ca.* 1590 cm^{-1}. This indicates the porous nature of the carbonaceous material, and is consistent with the previous report.[37] The X-ray diffraction (XRD) pattern shows a broad peak at 26.5° 2θ (Fig. S3b†) and, together with the Raman spectrum, confirms the characteristics of the carbonaceous material. This is in agreement with the data for doped carbon materials.[26] The surface composition analysis based on the survey X-ray photoelectron spectroscopy (XPS) spectrum (Fig. S4†) found that the as-prepared carbonaceous material consists of 92.5 at% C, 5.2 at% O and 2.3 at% N. The high-resolution C 1s spectrum in Fig. 1h was deconvoluted into four peaks, representing C–C/C=C at 284.6 eV, C–O/C–N at 285.6 eV, C=O at 287.4 eV and O–C=O at 289.1 eV.[27,40] This confirms both O and N functional groups exist in the obtained carbonaceous material. The high-resolution N 1s spectrum in Fig. 1i was deconvoluted into four peaks, corresponding to pyridinic N at 398.5 eV, pyrrolic N at 400.3 eV, quaternary N at 401.4 eV, and oxidized N at 402.6 eV.[41,42] The high-resolution O 1s spectrum in Fig. 1j was deconvoluted into three peaks, assigned to C=O (carboxyl) groups at 530.5 eV, C=O (ester, amides) groups at 532.3 eV, and COH, N–OC groups at 534.2 eV.[43]

This indicates the presence of various oxygen-containing functional groups with doubly and singly bound oxygen.

A polar carbonaceous surface, obtained through molecular functionalization or heteroatom doping, is essential for chemical bonding of the otherwise soluble polysulfides onto the carbon surface to minimize the shuttle effect. N-Doping has been extensively explored for this purpose.[24,25,28,36,44] However, the role of a small amount of oxygen heteroatom in carbonaceous materials converted from cellulose has not caught enough attention, although oxygen often exists in such carbonaceous materials. Wang *et al.*[45] reported that the presence of oxygen impurities, particularly those bonded to vacancies and edges, may stabilize lithium polysulfides. Our recent first principles-based calculations also suggest that O dopants, mainly through Li–O bonds, have significantly larger binding energy than N dopants due to the more electronegative nature of O compared to that of N and C. Furthermore, O- and N-dopants can also work synergistically to enhance the bonding of polysulfides on the carbon surface.[46] Therefore, the small amount of oxygen, present in addition to nitrogen in the soybean-derived hierarchical porous carbon, will improve stabilization of lithium polysulfides that may otherwise diffuse into the electrolyte.

To summarize, both the electron microscopy imaging and nitrogen adsorption results reveal a 3D hierarchical porous structure of the as-prepared soybean-derived carbonaceous material, which is suitable as a conductive matrix for sulfur loading and polysulfides confinement. In this hierarchical porous structure, sulfur species could be trapped in the micropores and result in enhanced electrochemical activity and reduced diffusion, whereas the mesopores serve as facile Li^+ transportation channels and provide buffer for volume expansion.[1] In addition to the physical confinement by micro- and meso-pores, chemical binding of polysulfides onto the O- and N-doped matrix surface is more effective in alleviating their shuttle effect as well as enabling the uniform distribution of sulfur species on the matrix surface during cycling.

The sulfur cathodes were prepared by drop-casting the cathode slurry into a freestanding edge-oriented multilayer graphene foam (GF) that was used as a current collector.[47] It has a mass density of less than *ca.* 1.5 mg cm^{-2}, which is much lower than the conventional aluminum current collector. Cells with Li chips to be used as anodes were assembled to study their electrochemical property and test their performance. They were investigated at different charge–discharge (C–D) current densities, ranging from 0.1 to 1C, over a potential window of 1.8–2.6 V *vs.* Li/Li^+. The specific capacity was calculated based on sulfur loading. The highly insulating sulfur particles may

introduce dead volume, whereas dissolution and re-deposition of sulfur species in the C–D process will not only cause the initial "bursting release" of polysulfides away from the cathode, but also could help to redistribute the active species more uniformly on the conducting carbon matrix in the cathode. Therefore, the initial activation process was investigated by performing electrochemical impedance spectroscopy (EIS) in the first few C–D cycles for a cell with a sulfur loading of 2.6 mg cm^{-2} at a 0.2C rate. The EIS measurement was conducted at the fully charged state (S_8 state) for each cycle. As shown in Fig. 2a, there was a relatively large discharge capacity loss after the first cycle, from 1130 to 1110 mA h g^{-1}. This was probably due to the initial "bursting release" of soluble polysulfides, and the formation of solid electrolyte interphase. After the first cycle, the capacity became relatively stable. Fig. 2b presents the EIS results and the fitting curves, obtained using the equivalent circuit shown in the inset. The intercept of impedance curve at the Z' axis represents the equivalent series resistance (R) that includes electronic resistance of electrode, ionic resistance of electrolyte, and contact resistance. The diameter of the semi-circle on the impedance curve indicates the charge-transfer resistance (R_{ct}), which represents the resistance of the electrochemical reaction on the interface of the electrolyte and electrode. The inclined line at low frequency means Warburg impedance (W), which corresponds to the diffusion of lithium ions. The fitted curves clearly indicate a dramatic decrease of R_{ct} after the first cycle, from 6.7 Ω cm^2 to 1.8 Ω cm^2. This suggests that the solid and insulating sulfur redistributed uniformly on the conductive matrix during electrochemical reaction that involves multistep solid–liquid–solid conversions. CV scans at 0.1 mV s^{-1} were conducted on another fresh cell for the first few cycles, as shown in Fig. 2d. All peaks on the CV curves become sharper and are stable after the first cycle, whereas the anodic peaks shift to a higher voltage. This is consistent with the results obtained from the C–D curves.

Fig. 3 represents the results from cells with a sulfur loading of 2.0 mg cm^{-2}. In Fig. 3a, the initial discharge capacity at 0.1C was as high as 1330 mA h g^{-1}. This indicates high sulfur utilization. Afterwards, the cells displayed stable specific capacities of 1300, 1120, 870, and 710 mA h g^{-1} at 0.1, 0.2, 0.5, and 1C, respectively. After cycling at different current densities, the specific capacity did not suffer any obvious loss when the current returned to 0.1C. The C–D profiles at different C–D rates acquired for the fifth C–D cycle, *i.e.*, after the profiles were stable at each rate, are plotted in Fig. 3b. The discharge profiles exhibit two plateaus and two slopes. As proposed in ref. 48, the high plateau at *ca.* 2.38 V on the discharge curve at 0.1C corresponds to the first reduction step of sulfur to long chain polysulfides such as S_8^- and S_6^-, whereas the slope that follows is the second reduction step with a gradual reduction of polysulfide chain lengths, producing mainly S_4^-. The low plateau at *ca.* 2.10 V corresponds to a further chain reduction to short polysulfide species such as S_2^{2-} and S^{2-}. The precipitation of these poorly soluble and highly insulating Li_2S_2 and Li_2S compounds leads to electrode passivation with a gradual ending of discharge. The charge profile also exhibits two plateaus, but

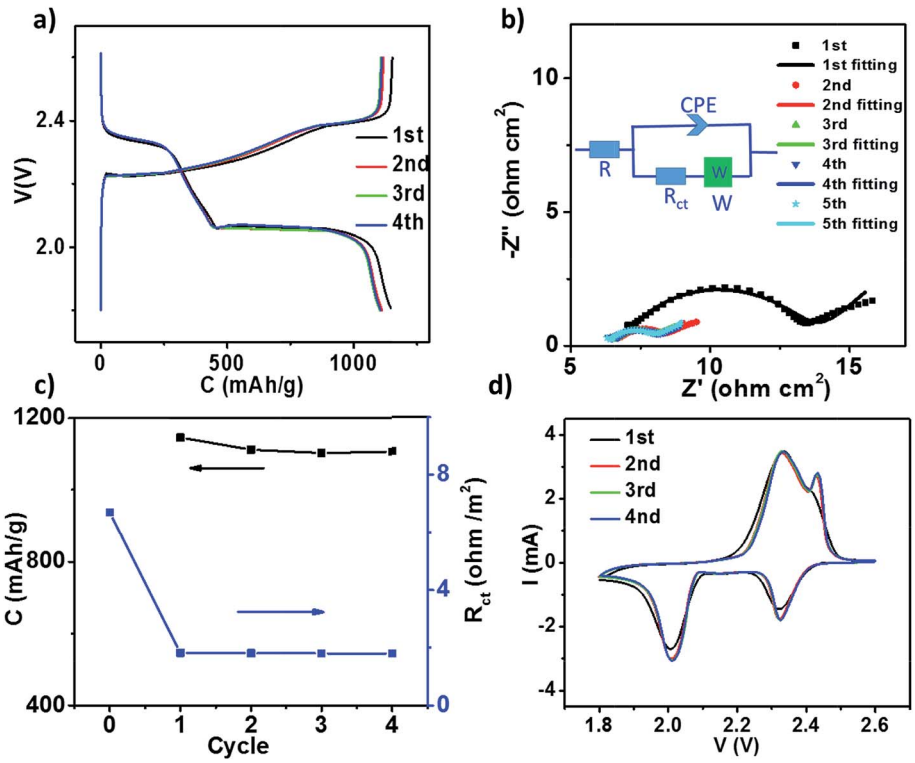

Fig. 2 (a) The behavior of the first few cycles at 0.2C of a cell, and (b) the Nyquist plot of the same cell from the EIS measurement before discharge and after each discharge–charge cycle at 2.6 V; (c) specific capacity and charge transfer resistant evolution in the first few cycles. (d) CV behavior for a typical cell in the first few CV cycles measured at 0.1 mV s^{-1}.

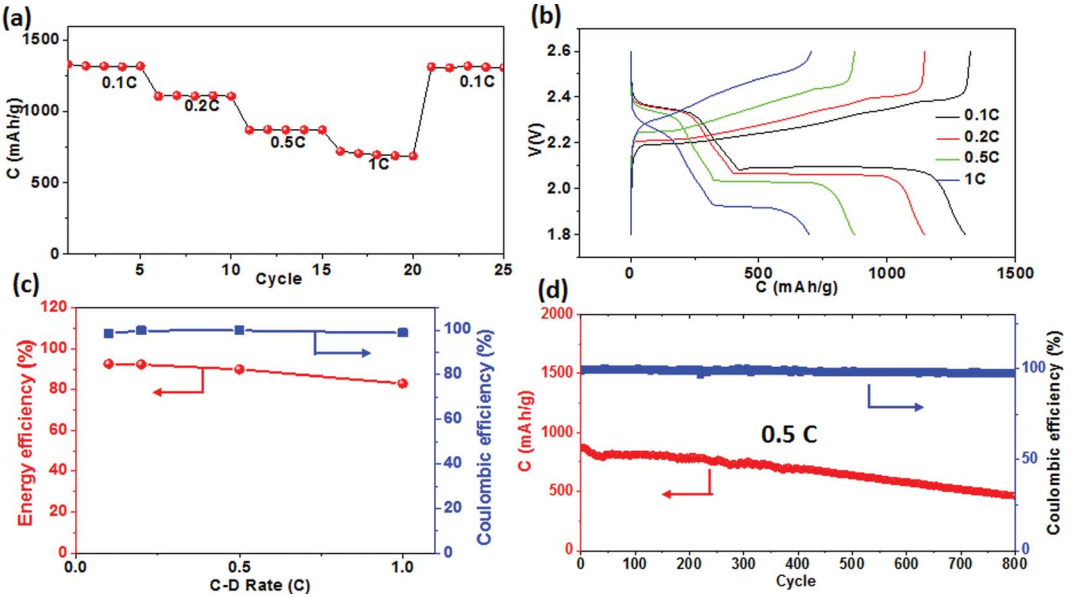

Fig. 3 (a) Specific capacity at different discharge rates; (b) the fifth C–D curves at different C–D rates; (c) energy efficiency and coulombic efficiency for the fifth C–D cycle at different C–D rates; (d) cyclability test at 0.5C for 800 cycles.

these plateaus are not as prominent as the plateaus for the discharge profile. The separation between charge and discharge potentials increases with current density due to polarization loss. Similar observation can be made from the CV measurement (Fig. S5†) that shows two well-separated cathodic peaks and two closely-spaced anodic peaks, with the cathodic and anodic peaks shift due to polarization at higher scan rates. Coulombic efficiency and energy efficiency from the fifth C–D curves at each rate are plotted in Fig. 3c. The cells exhibited a high coulombic efficiency of *ca.* 99% for all the measured rates. This suggests a weak shuttle effect. Energy efficiency is a more important parameter when considering energy storage and consumption, but it is unfortunately not reported in most publications. At 0.1 and 0.2C, our cells exhibited a high energy efficiency of *ca.* 92%. At 0.5 and 1C, the cells had energy efficiency of 89% and 82%, respectively. We believe that the excellent performance of the sulfur electrode is due to the synergistic effect of hierarchical porous structure and heteroatom doping in the soybean-derived carbonaceous material. The hierarchical porous structure with a large specific surface area facilitates the uniform distribution of sulfur species in the carbon matrix during electrochemical reactions, favors electrolyte penetration into electrode matrix, and physically confines soluble lithium polysulfides, whereas O- and N-dopants render carbon surface strongly adsorbing the otherwise soluble lithium polysulfides and reduce the charge transfer barrier in the electrochemical reactions. The synergetic physical and chemical effects from this unique carbon material collaboratively contribute to the high performance of the sulfur electrode that contains this material in an LSB cell. The excellent stability was further investigated by the long-term cycling test. Three cells with a sulfur loading of 2.0 mg cm^{-2} were cycled at 0.1C for 150 cycles, 0.2C for 700 cycles, 0.5C for 800 cycles (Fig. 3d and S6†). These cells had the final capacity of 1020, 640, and 460 mA h g^{-1} and the capacity retention of 78%, 57%, and 53%, respectively.

To further demonstrate the practical potential of the as-prepared soybean-derived carbonaceous material, cells with a high sulfur loading of 5.5 mg cm^{-2} were assembled to achieve a high areal capacity. This is vital for commercializing LSBs since the conventional lithium-ion batteries typically have an areal capacity (C_A) of 4–5 mA h cm^{-2}. For most cathode designs, the specific capacity will significantly decrease at a higher sulfur loading because a larger portion of the polysulfides will diffuse away; most publications have therefore reported a low sulfur loading, typically approximately 2 mg cm^{-2} or less. However, our cells with a sulfur loading as high as 5.5 mg cm^{-2} still displayed high specific capacities of 1200, 1070, 970 and 710 mA h g^{-1} at 0.05, 0.1, 0.2 and 0.5C, respectively. These correspond to areal capacities of 6.6, 5.9, 5.3 and 3.9 mA h cm^{-2} (Fig. 4a and b), and are comparable with the areal capacity of practical lithium-ion batteries. The cell was cycled at 0.2C and 81% of its initial capacity was maintained after 100 cycles (Fig. 4c and d). Since the stability of LSB cells depends on both the sulfur cathode and the lithium anode, the failed cell (Fig. S7†) was disassembled for inspection to reveal the degradation and failure mechanisms of the high-loading cells. From a photograph and SEM images (Fig. S8†), no evident change was found in the cathode; however, the lithium metal anode was severely eroded and a thick solid electrolyte interphase (SEI) layer had formed on the surface. Thus, the capacity fading was more likely caused by lithium corrosion and electrolyte decomposition and depletion,[49] rather than a considerable degradation of the sulfur cathode. An improved Li anode design would further enhance the electrochemical stability of the cells with a high sulfur loading. Although further progress is needed, we emphasize that the cathode design based on the soybean-derived hierarchical porous carbon with intrinsic heteroatom dopants shows a better overall

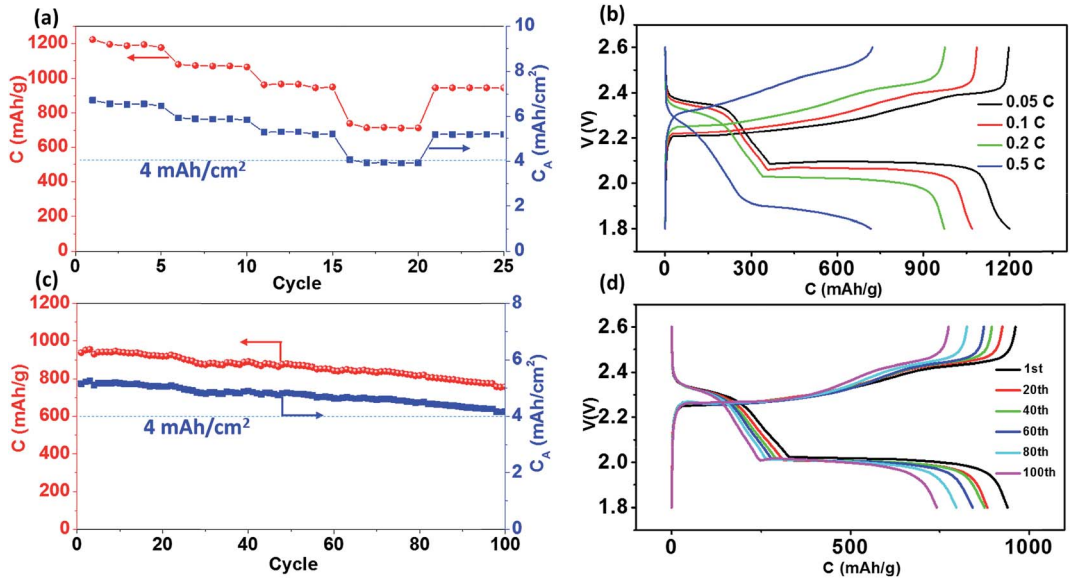

Fig. 4 Cell performance with a high sulfur loading of 5.5 mg cm^{-2}. (a) Specific capacity at different discharge rates; (b) C–D curves at different C–D rates; (c) cyclability test at 0.2C; (d) selected C–D profiles.

performance than many reported nitrogen-doped carbon-based designs.[24,50–52] Considering its large areal capacity, high sulfur loading and utilization, and good stability, this material represents significant progress toward the practical application of LSBs. The excellent performance of the battery described herein, prepared using cheap materials and easy processes moves the LSBs a step closer to practical application.

3. Conclusion

In this study, a simple pyrolysis/activation process was employed to derive a hierarchical porous carbon nanostructure from crude soybeans. Its ultrahigh specific surface area of *ca.* 1500 m^2 g^{-1} with dominant micropores can enhance the confinement of soluble polysulfides, whereas the intrinsic O- and N-dopants synergistically contribute to the chemical binding of polysulfides as well as reducing the electron transfer resistance during electrochemical conversion. As a result, sulfur electrodes with a high sulfur content, large sulfur mass loading, and excellent performance can be fabricated using this new material. Cells with such sulfur cathodes demonstrated large capacity, high coulombic and energy efficiencies, and high cycling stability. For a sulfur loading of 5.5 mg cm^{-2}, cells displayed a specific capacity of *ca.* 950 mA h g^{-1} at 0.2C, which corresponds to an areal capacity of 5.2 mA h cm^{-2}. It is envisioned that with a better lithium anode design, application of the cathode developed in this study will move the LSB technology a step closer to being practical.

4. Experiments

Preparation of soybean-derived activated carbon

30 g of original soybeans, without being crushed into powder, was first sealed into a 100 mL Teflon-lined autoclave, and then heated at 180 °C for 20 h. To produce activated carbon, 20 g of the obtained soybean black paste was mixed with KOH in a mass ratio of 1 : 1, and then 20 mL deionized water was added to make a uniform slurry by stirring. The slurry was dried at 120 °C in vacuum to obtain the uniformly mixed soybeans and KOH. This mixture was pyrolyzed at 800 °C in an argon environment for 2 h with a heating rate of 2.5 K min^{-1}. The pyrolyzed product was washed in dilute HCl a few times, and then in deionized water repeatedly to remove ion impurities. The final soybean-derived activated carbon product was obtained by drying the washed product at 80 °C in vacuum overnight.

Material characterization

The morphology and the hierarchical porous structure of the soybean-derived activated carbon were revealed by a LEO field emission scanning electron microscope (SEM) and a Hitachi H-9500 transmission electron microscope (TEM). The surface elemental composition and chemical bonding were analyzed using a Physical Electronics PHI 5000 VersaProbe X-ray photoelectron spectrometer (XPS) with photoelectrons excited by monochromatic Al K_α radiation (1486.6 eV). The survey scans in the 0–1400 eV binding energy (BE) range were collected with a pass energy of 187.85 eV and a step of 0.8 eV. For the high-resolution scans, the pass energy was 23.5 eV with a step of 0.1 eV. The C 1s, O 1s and N 1s core level spectra were fitted using Physical Electronics PHI MultiPak software with a Gaussian sum function, a Shirley background subtraction and an iterative least-squares optimization algorithm. To correct for sample charging, the BE of the spectra was referenced to the C–C peak C 1s spectrum with BE at 284.6 eV.[24] Before the XPS measurement, the sample was dried at 60 °C in vacuum overnight to remove the adsorbed water. The Raman spectrum was recorded on a Bruker Optics Senterra dispersive Raman microscope spectrometer with a spectral resolution of ~3–5 cm^{-1} using 532 nm laser excitation.

The X-ray powder diffraction (XRD) pattern was obtained using a Philips X'Pert system. The nitrogen adsorption measurement was conducted at 77 K using a Quantachrome Autosorb iQ (ASiQ) micropore analyzer. The sample was outgassed at 150 °C for 18 h under high vacuum. The multi-point specific surface area (S_{BET}) was determined from the adsorption isotherm using the Brunauer–Emmett–Teller (BET) method. The pore size distribution was calculated from the nitrogen adsorption data using a non-local density functional theory N_2/carbon equilibrium transition kernel at 77 K based on a slit-pore model.

Electrode fabrication and electrochemical measurements

The active S/C composite with sulfur loading of 80 wt% was made by mixing sulfur and the soybean-derived activated carbon. These components were mixed in a mass ratio of 4 : 1 (S : C) by manually grinding for 1 h in mortar using a pestle. The mixture was then sealed in a Teflon-lined autoclave and heated at 155 °C for 12 h, so that sulfur and the activated carbon could be well mixed. The cathode paste was then made by adding 20 wt% carbon black, and 10 wt% polyvinylidenefluoride (PVDF) binder. The S/C composite was mixed with carbon black by grinding together, while PVDF was dissolved in *N*-methylpyrrolidone (NMP) solvent using magnetic stirring until the solution was uniform. Then, the ground mixture was transferred into the solution, and stirred continuously for a few hours until a uniform slurry was obtained. To fabricate the cathode, the slurry was drop-casted onto freestanding edge-oriented graphene (EOG) foam and dried at 60 °C for 20 h. The EOG foam used was obtained by EOG growth inside a sacrificial Ni foam.[53,54] It has a mass density of less than *ca.* 1.5 mg cm^{-2}, much lower than the commonly used Al current collector, *e.g.*, 14.9 μm thick, 4.02 mg cm^{-2}. The as-prepared cathodes were assembled into coin cells in an Ar-filled Vigor glovebox where oxygen and moisture are both held below 1 ppm. Lithium chips were used as the anode. Separators were soaked with electrolyte that consisted of 1.0 M bis(trifluoromethane)sulfonimide lithium salt (LiTFSI) in a mixed solvent of 1,2-dimethoxyethane (DME) and 1,3-dioxolane (DOL) (1 : 1, v/v) with 2 wt% lithium nitrate ($LiNO_3$) as an additive. The ratio of the volume (μL) of the electrolyte to the mass (mg) of sulfur was controlled at 15 : 1. The newly-assembled cells were stored for 12 h before testing, allowing electrolyte diffusion into the cathode. Cell characterization was carried out using cyclic voltammetry (CV), charge–discharge (C–D), and electrochemical impedance spectroscopy (EIS). C–D tests were conducted with a Land CT2001A battery test system at different current densities over a voltage window of 1.8–2.6 V. CV tests were executed using a Biologic SP-150 electrochemical workstation at different scan rates from 0.05 mV s^{-1} to 0.2 mV s^{-1}. EIS was measured in the frequency range from 1 MHz to 0.1 Hz with a sinusoidal signal of 10 mV at an open circuit potential of 2.6 V.

References

1 A. Manthiram, Y. Fu, S.-H. Chung, C. Zu and Y.-S. Su, Rechargeable lithium–sulfur batteries, *Chem. Rev.*, 2014, **114**, 11751–11787.
2 J.-G. Wang, K. Xie and B. Wei, Advanced engineering of nanostructured carbons for lithium–sulfur batteries, *Nano Energy*, 2015, **15**, 413–444.
3 X. Ji, S. Evers, R. Black and L. F. Nazar, Stabilizing lithium–sulphur cathodes using polysulphide reservoirs, *Nat. Commun.*, 2011, **2**, 325.
4 R. Xu, J. C. Li, J. Lu, K. Amine and I. Belharouak, Demonstration of highly efficient lithium–sulfur batteries, *J. Mater. Chem. A*, 2015, **3**, 4170–4179.
5 C. Huang, J. Xiao, Y. Shao, J. Zheng, W. D. Bennett, D. Lu, L. V. Saraf, M. Engelhard, L. Ji and J. Zhang, Manipulating surface reactions in lithium–sulphur batteries using hybrid anode structures, *Nat. Commun.*, 2014, **5**, 3015.
6 Y.-S. Su, Y. Fu, T. Cochell and A. Manthiram, A strategic approach to recharging lithium–sulphur batteries for long cycle life, *Nat. Commun.*, 2013, **4**, 2985.
7 K. Liao, P. Mao, N. Li, M. Han, J. Yi, P. He, Y. Sun and H. Zhou, Stabilization of polysulfides *via* lithium bonds for Li–S batteries, *J. Mater. Chem. A*, 2016, **4**, 5406–5409.
8 A. Rosenman, E. Markevich, G. Salitra, D. Aurbach, A. Garsuch and F. F. Chesneau, Review on Li–sulfur battery systems: An integral perspective, *Adv. Energy Mater.*, 2015, **5**, 1500212.
9 M. R. Busche, P. Adelhelm, H. Sommer, H. Schneider, K. Leitner and J. Janek, Systematical electrochemical study on the parasitic shuttle-effect in lithium–sulfur-cells at different temperatures and different rates, *J. Power Sources*, 2014, **259**, 289–299.
10 T. Zhang, M. Marinescu, L. O'Neill, M. Wild and G. Offer, Modeling the voltage loss mechanisms in lithium–sulfur cells: the importance of electrolyte resistance and precipitation kinetics, *Phys. Chem. Chem. Phys.*, 2015, **17**, 22581–22586.
11 R. Xu, J. Lu and K. Amine, Progress in mechanistic understanding and characterization techniques of Li–S batteries, *Adv. Energy Mater.*, 2015, **5**, 1500408.
12 H. Li, X. Yang, X. Wang, M. Liu, F. Ye, J. Wang, Y. Qiu, W. Li and Y. Zhang, Dense integration of graphene and sulfur through the soft approach for compact lithium/sulfur battery cathode, *Nano Energy*, 2015, **12**, 468–475.
13 X. Ji, K. T. Lee and L. F. Nazar, A highly ordered nanostructured carbon–sulphur cathode for lithium–sulphur batteries, *Nat. Mater.*, 2009, **8**, 500–506.
14 Z. W. Seh, W. Li, J. J. Cha, G. Zheng, Y. Yang, M. T. McDowell, P.-C. Hsu and Y. Cui, Sulphur–TiO_2 yolk–shell nanoarchitecture with internal void space for long-cycle lithium–sulphur batteries, *Nat. Commun.*, 2013, **4**, 1331.
15 Q. Pang, D. Kundu, M. Cuisinier and L. Nazar, Surface-enhanced redox chemistry of polysulphides on a metallic and polar host for lithium–sulphur batteries, *Nat. Commun.*, 2014, **5**, 4759.
16 X. Liang, C. Hart, Q. Pang, A. Garsuch, T. Weiss and L. F. Nazar, A highly efficient polysulfide mediator for lithium–sulfur batteries, *Nat. Commun.*, 2015, **6**, 5682.
17 X. Liang, Z. Wen, Y. Liu, M. Wu, J. Jin, H. Zhang and X. Wu, Improved cycling performances of lithium–sulfur batteries

with $LiNO_3$-modified electrolyte, *J. Power Sources*, 2011, **196**, 9839–9843.

18 J. R. Nair, F. Bella, N. Angulakshmi, A. M. Stephan and C. Gerbaldi, Nanocellulose–laden composite polymer electrolytes for high performing lithium–sulphur batteries, *Energy Storage Materials*, 2016, **3**, 69–76.

19 F. Wu, J. T. Lee, N. Nitta, H. Kim, O. Borodin and G. Yushin, Lithium iodide as a promising electrolyte additive for lithium–sulfur batteries: mechanisms of performance enhancement, *Adv. Mater.*, 2015, **27**, 101–108.

20 R. Cao, W. Xu, D. Lv, J. Xiao and J. G. Zhang, Anodes for rechargeable lithium–sulfur batteries, *Adv. Energy Mater.*, 2015, **5**, 1042273.

21 A. C. Kozen, C.-F. Lin, A. J. Pearse, M. A. Schroeder, X. Han, L. Hu, S.-B. Lee, G. W. Rubloff and M. Noked, Next-generation lithium metal anode engineering *via* atomic layer deposition, *ACS Nano*, 2015, **9**, 5884–5892.

22 N. Jayaprakash, J. Shen, S. S. Moganty, A. Corona and L. A. Archer, Porous Hollow Carbon@Sulfur Composites for High-Power Lithium–Sulfur Batteries, *Angew. Chem.*, 2011, **123**, 6026–6030.

23 J. Guo, Y. Xu and C. Wang, Sulfur-impregnated disordered carbon nanotubes cathode for lithium–sulfur batteries, *Nano Lett.*, 2011, **11**, 4288–4294.

24 J. Song, T. Xu, M. L. Gordin, P. Zhu, D. Lv, Y. B. Jiang, Y. Chen, Y. Duan and D. Wang, Nitrogen-doped mesoporous carbon promoted chemical adsorption of sulfur and fabrication of high-areal-capacity sulfur cathode with exceptional cycling stability for lithium–sulfur batteries, *Adv. Funct. Mater.*, 2014, **24**, 1243–1250.

25 J. Song, M. L. Gordin, T. Xu, S. Chen, Z. Yu, H. Sohn, J. Lu, Y. Ren, Y. Duan and D. Wang, Strong lithium polysulfide chemisorption on electroactive sites of nitrogen-doped carbon composites for high-performance lithium–sulfur battery cathodes, *Angew. Chem., Int. Ed.*, 2015, **54**, 4325–4329.

26 J. Zhang, Y. Cai, Q. Zhong, D. Lai and J. Yao, Porous nitrogen-doped carbon derived from silk fibroin protein encapsulating sulfur as a superior cathode material for high-performance lithium–sulfur batteries, *Nanoscale*, 2015, **7**, 17791–17797.

27 G. Zhou, E. Paek, G. S. Hwang and A. Manthiram, Long-life Li/polysulphide batteries with high sulphur loading enabled by lightweight three-dimensional nitrogen/sulphur-codoped graphene sponge, *Nat. Commun.*, 2015, **6**, 7760.

28 C. Tang, Q. Zhang, M. Q. Zhao, J. Q. Huang, X. B. Cheng, G. L. Tian, H. J. Peng and F. Wei, Nitrogen-doped aligned carbon nanotube/graphene sandwiches: Facile catalytic growth on bifunctional natural catalysts and their applications as scaffolds for high-rate lithium–sulfur batteries, *Adv. Mater.*, 2014, **26**, 6100–6105.

29 X. Tao, J. Wang, C. Liu, H. Wang, H. Yao, G. Zheng, Z. W. Seh, Q. Cai, W. Li and G. Zhou, Balancing surface adsorption and diffusion of lithium–polysulfides on nonconductive oxides for lithium–sulfur battery design, *Nat. Commun.*, 2016, **7**, 11203.

30 X. Liang, C. Y. Kwok, F. Lodi-Marzano, Q. Pang, M. Cuisinier, H. Huang, C. J. Hart, D. Houtarde, K. Kaup and H. Sommer, Tuning Transition Metal Oxide–Sulfur Interactions forLong Life Lithium–Sulfur Batteries: The "Goldilocks" Principle, *Adv. Energy Mater.*, 2015, **6**, 1501636.

31 G. Zheng, Q. Zhang, J. J. Cha, Y. Yang, W. Li, Z. W. Seh and Y. Cui, Amphiphilic surface modification of hollow carbon nanofibers for improved cycle life of lithium–sulfur batteries, *Nano Lett.*, 2013, **13**, 1265–1270.

32 S. Li, T. Mou, G. Ren, J. Warzywoda, B. Wang and Z. Fan, Confining Sulfur Species in Cathodes of Lithium–Sulfur Batteries: Insight into Nonpolar and Polar Matrix Surfaces, *ACS Energy Lett.*, 2016, **1**, 481–489.

33 G. Li, J. Sun, W. Hou, S. Jiang, Y. Huang and J. Geng, Three-dimensional porous carbon composites containing high sulfur nanoparticle content for high-performance lithium–sulfur batteries, *Nat. Commun.*, 2016, **7**, 10601.

34 R. Fang, S. Zhao, P. Hou, M. Cheng, S. Wang, H. M. Cheng, C. Liu and F. Li, 3D Interconnected Electrode Materials with Ultrahigh Areal Sulfur Loading for Li–S Batteries, *Adv. Mater.*, 2016, **28**, 3374–3382.

35 L. Qie, C. Zu and A. Manthiram, A High Energy Lithium–Sulfur Battery with Ultrahigh-Loading Lithium Polysulfide Cathode and its Failure Mechanism, *Adv. Energy Mater.*, 2016, **6**, 1502459.

36 J. Song, Z. Yu, M. L. Gordin and D. Wang, Advanced Sulfur Cathode Enabled by Highly Crumpled Nitrogen-doped Graphene Sheets for High-Energy-Density Lithium–Sulfur Batteries, *Nano Lett.*, 2015, **16**, 864–870.

37 M. Wahid, G. Parte, D. Phase and S. Ogale, Yogurt: a novel precursor for heavily nitrogen doped supercapacitor carbon, *J. Mater. Chem. A*, 2015, **3**, 1208–1215.

38 M. Wahid, D. Puthusseri, D. Phase and S. Ogale, Enhanced capacitance retention in a supercapacitor made of carbon from sugarcane bagasse by hydrothermal pretreatment, *Energy Fuels*, 2014, **28**, 4233–4240.

39 J. W. To, Z. Chen, H. Yao, J. He, K. Kim, H.-H. Chou, L. Pan, J. Wilcox, Y. Cui and Z. Bao, Ultrahigh Surface Area Three-Dimensional Porous Graphitic Carbon from Conjugated Polymeric Molecular Framework, *ACS Cent. Sci.*, 2015, **1**, 68–76.

40 W. Luo, B. Wang, C. G. Heron, M. J. Allen, J. Morre, C. S. Maier, W. F. Stickle and X. Ji, Pyrolysis of cellulose under ammonia leads to nitrogen-doped nanoporous carbon generated through methane formation, *Nano Lett.*, 2014, **14**, 2225–2229.

41 X. Wang, Z. Zhang, Y. Qu, Y. Lai and J. Li, Nitrogen-doped graphene/sulfur composite as cathode material for high capacity lithium–sulfur batteries, *J. Power Sources*, 2014, **256**, 361–368.

42 H. Wang, T. Maiyalagan and X. Wang, Review on recent progress in nitrogen-doped graphene: synthesis, characterization, and its potential applications, *ACS Catal.*, 2012, **2**, 781–794.

43 W. Shen, Z. Li and Y. Liu, Surface chemical functional groups modification of porous carbon, *Recent Pat. Chem. Eng.*, 2008, **1**, 27–40.

44 Y. Qiu, W. Li, W. Zhao, G. Li, Y. Hou, M. Liu, L. Zhou, F. Ye, H. Li, Z. Wei, S. Yang, W. Duan, Y. Ye, J. Guo and Y. Zhang, High-rate, ultralong cycle-life lithium/sulfur batteries enabled by nitrogen-doped graphene, *Nano Lett.*, 2014, **14**, 4821–4827.

45 B. Wang, S. M. Alhassan and S. T. Pantelides, Formation of large polysulfide complexes during the lithium–sulfur battery discharge, *Phys. Rev. Appl.*, 2014, **2**, 034004.

46 S. Li, T. Mou, G. Ren, J. Warzywoda, Z. Wei, B. Wang and Z. Fan, Sulfur Cathodes Based on Carbon Nanoribbon Aerogel with Simultaneously High Sulfur Content and Large Mass Loading for High-Performance Lithium–Sulfur Batteries, in review.

47 G. Ren, M. N. F. Hoque, J. Liu, J. Warzywoda and Z. Fan, Perpendicular edge oriented graphene foam supporting orthogonal TiO_2 (B) nanosheets as freestanding electrode for lithium ion battery, *Nano Energy*, 2016, **21**, 162–171.

48 C. Barchasz, F. Molton, C. Duboc, J.-C. Leprêtre, S. Patoux and F. Alloin, Lithium/sulfur cell discharge mechanism: an original approach for intermediate species identification, *Anal. Chem.*, 2012, **84**, 3973–3980.

49 L. Qie, C. Zu and A. Manthiram, A high energy lithium–sulfur battery with ultrahigh-loading lithium polysulfide cathode and its failure mechanism, *Adv. Energy Mater.*, 2016, **6**, 1502469.

50 Y. Qu, Z. Zhang, X. Zhang, G. Ren, Y. Lai, Y. Liu and J. Li, Highly ordered nitrogen-rich mesoporous carbon derived from biomass waste for high-performance lithium–sulfur batteries, *Carbon*, 2015, **84**, 399–408.

51 Z. Zhang, G. Wang, Y. Lai, J. Li, Z. Zhang and W. Chen, Nitrogen-doped porous hollow carbon sphere-decorated separators for advanced lithium–sulfur batteries, *J. Power Sources*, 2015, **300**, 157–163.

52 C. Wang, K. Su, W. Wan, H. Guo, H. Zhou, J. Chen, X. Zhang and Y. Huang, High sulfur loading composite wrapped by 3D nitrogen-doped graphene as a cathode material for lithium–sulfur batteries, *J. Mater. Chem. A*, 2014, **2**, 5018–5023.

53 G. Ren, M. N. F. Hoque, X. Pan, J. Warzywoda and Z. Fan, Vertically aligned VO_2 (B) nanobelt forest and its three-dimensional structure on oriented graphene for energy storage, *J. Mater. Chem. A*, 2015, **3**, 10787–10794.

54 G. Ren, X. Pan, S. Bayne and Z. Fan, Kilohertz ultrafast electrochemical supercapacitors based on perpendicularly-oriented graphene grown inside of nickel foam, *Carbon*, 2014, **71**, 94–101.